H2O-fluid-saturated melting of subducted continental crust facilitates exhumation of ultrahigh-pressure rocks in continental subduction zones

Loic Labrousse, T. Duretz, T. Gerya

H_2O-fluid-saturated melting of subducted continental crust facilitates exhumation of ultrahigh-pressure rocks in continental subduction zones

L. Labrousse (1,2), T. Duretz (3), T. Gerya (4)

1- Sorbonne Universités, UPMC Univ Paris 06, CNRS, ISTEP, case 129, 4, place Jussieu, F-75005 PARIS, loic.labrousse@upmc.fr

2- Takuvik joint International Laboratory, Université Laval-CNRS (France), Département de Géologie et Génie Géologique, Université Laval, Canada

3-Institut des sciences de la Terre, UNIL Lausanne, Switzerland

4-Institute of Geophysics, ETH-Zürich, Zürich, Switzerland

Abstract

We present two-dimensional numerical models of plate subduction and collision inspired by the Scandinavian Caledonian orogeny to investigate the possible impact of continental crust partial melting on the exhumation of Ultra-High Pressure metamorphic rocks. Three possible reactions were tested: low temperature solidus representing H_2O-fluid-saturated partial melting, and two end-member reaction curves for dehydration melting. Thermo-mechanical effects of partial melting were implemented as (1) a viscosity decrease as a determined rheologically critical melt percentage was reached (here 0.1), (2) a change in effective heat capacity and adiabatic heating/cooling accounting for a latent heat term in the heat equation. Among the 3 tested reactions, only H_2O-fluid-saturated partial melting drastically modifies the collision dynamics from the non-melting reference model holding all other parameters constant. A substantially low general viscosity trunction (here 10^{17} Pa.s) is needed to properly resolve the effect of partial melting on deep collision processes. Low temperature melting indeed induces the development of a low viscosity buoyant plume prior to slab detachment, where migmatites exhume from UHP conditions at rates and with pressure-temperature paths similar to the natural values acknowledged for the Norwegian Caledonides. High temperature melting has no drastic influence on early collision dynamics. While positive buoyancy remains the first order driver for the exhumation of buried continental rocks, exhumation initiates in these cases with eduction subsequent to slab detachment. Melting and formation of a migmatite plume can later occur along decompression path while continental crust undergoes thermal reequilibration at temperatures above 900°C. Some of the partially molten material can also relaminate in the overriding plate rather than exhume within the collision zone. Even if minor in terms of amount of magma produced, H_2O-fluid-saturated partial melting at UHP conditions could therefore have a dramatic rheological effect and actually limits continental rocks subduction and facilitates their exhumation.

Keywords

UltraHigh Pressure metamorphism, partial melting, continental subduction

Highlights

- Partial melting of continental crust influences early subduction collision dynamics.
- H_2O-fluid-saturated partial melting can explain specific exhumation history of the Norwegian Caledonides migmatite-bearing ultra-high pressure rocks.

- Partial melting of the crust and slab detachment both limit continental subduction.

1. Introduction

Partial melting is considered as a first order weakening mechanism for continental crust based on experimental evidences (Rosenberg, 2001). While most studies infer a rheologically critical melt percentage (RCMP), beyond which migmatites are sensitively weaker than their protolith, values for this threshold vary from 7 up to 20 percents according to experiments (Rosenberg and Handy, 2005). In the Scandinavian Caledonides, some of the (Ultra) High Pressure, (U)HP bearing Western Gneiss (WGR) show migmatization associated to their exhumation, whereas others do not (Labrousse et al., 2002; Hacker et al., 2010; Kylander-Clark et al., 2014). Whether partial melting occurs via dehydration melting (Auzanneau et al., 2006) or at least begun in the presence of free fluids (Ganzhorn et al., 2014) is a key issue. H_2O-fluid-saturated melting indeed could occur as early as the pressure peak assessed for the UHP eclogites (Labrousse et al., 2011) while dehydration reactions are crossed along retrograde path only. Sources for aqueous fluids in the 2.5-5 GPa pressure range within a subduction wedge are actually diverse (nominally anhydrous minerals, mantle hydrous phases breakdown) and fluid saturated melting is considered as a relevant reaction in these conditions. First increments of H_2O-fluid-saturated melting at peak conditions could act as a first weakening mechanism prone to decouple fertile continental crust from subjacent dry crust and mantle, hence triggering the exhumation of buoyant partially molten crust (Labrousse et al., 2011).

In this paper, we employ previously designed subduction-collision numerical models (Duretz et al., 2012a) to simulate the Caledonian collision event and Western Gneiss UHP province metamorphic history. We evaluate the impact of different partial melting reactions on the dynamics of UHP rocks exhumation, with emphasis on the exhumation rates and PT paths of UHP continental units. Possible relations between crustal partial melting and lithospheric delamination are also discussed.

2. Geological evidence of relations between UHP metamorphics exhumation and partial melting

All UHP metamorphic domains worlwide (Figure 1) share clockwise PT paths with peak pressure and temperature reached coevally in the coesite stability field. Nevertheless the shape of these paths and their position relative to relevant melting curves differ. In the Dabie Shan, Late Triassic- Early Jurassic partial melting occurred in the Central Dabie Shan migmatite UHP eclogite-bearing dome (Faure et al., 2003) which has a PT path (CDD, Figure 1) significantly hotter than other UHP units in the area, with an initial isothermal decompression path portion. In the Kokchetav Massif, Kazakhstan, UHP gneisses show compositions consistent with melt extraction (Shatsky et al., 1999). Dehydration melting reaction producing garnet in the coesite stability field is expected to occur according to documented PT path (Hermann et al., 2001). Zircon domains attributed to peak and early decompression stages (domain 2, Hermann et al., 2001) show REE patterns in equilibrium with restitic garnet, which is compatible with partial melting from the very first stages of exhumation, i.e. peak pressure. In the Erzgebirge, Bohemian Massif, coesite and diamond-bearing gneisses (Massonne, 2003) were exhumed from pressures higher than 4.5 GPa. Diamonds included in UHP garnets are interpreted as cristallized from a silicate melt (Massonne, 2003) and polyphase inclusions are interpreted as hydrous melts trapped in UHP conditions (Ferrero et al., 2015). In the WGR (Norwegian Caledonides, leucosome abundance is rising from south (SWGR, Figure 1) where lower pressure UHP eclogites are mostly exhumed within unmolten gneiss, to north (NWGR, Figure 1) where diamond bearing UHP eclogites are exhumed within pervasively molten gneiss (Hacker et al., 2010; Kylander-Clark and Hacker, 2014). Zircon ages from leucosomes overlap with age interval for UHP peak metamorphism (Gordon et al., 2013). Polycrystalline inclusions in eclogitic rims of garnets (Ganzhorn et al., 2014) evidence presence of silica-rich fluid at peak conditions and composition of early leucosomes are compatible with partial melting at UHP conditions (Labrousse et al., 2011). In the North Eastern Greenland eclogite province (NEGEP), partial melting of gneiss occurred in the coesite stability field (Lang and Gilotti, 2007) via phengite destabilization. Peak PT estimates are close to phengite dehydration reaction (Hermann et al., 2006). Partial melting on the retrograde path is also recorded (Gilotti and McClelland, 2007), and could be due to early retrograde garnet-producing reactions such as the one experimentally identified by Auzanneau et al. (2006). In the Sulu Orogen coesite-bearing zircons in gneiss showing evidence of equilibration with a melt yield ages clustering between 220 and 230 Ma, while peak metamorphism age is considered as 245-225 Ma in age (Hacker et al., 1998; Liu et al., 2012), meaning that partial melting occurred along the very first increments of retrograde path and promoted the exhumation of UHP metamorphics.

On the other hand, some UHP terranes did not undergo partial melting. In the Alps, Lago di Cignana unit, Zermatt-Saas Zone, which is the sole UHP unit with oceanic affinities (Reinecke, 1998) and Dora Maira Brossasco-Val Gilba unit, which is a kilometre-size metagranitic unit (Chopin and Schertl, 1999) both exhibit a cold peak metamorphism, and no evidence of partial melting. Southern Dabie Chan complex, which is considered as an intruded metasedimentary complex unit thrust on top of a UHP free gneiss unit (Hacker et al., 2000) show interaction with fluids at UHP (Xia et al., 2008) but no direct evidence of partial melting.

Compilation of PT paths from UHP metamorphic units shows that those exhibiting migmatites cross one experimental solidus curve at or close to their peak pressure, and that their first exhumation stages systematically occur via isothermal decompression (Figure 1). This specificity has been explained by adiabatic behaviour during fast exhumation of the top of the continental panel (Hermann et al., 2001) when lithospheric slab detaches. No systematic difference in exhumation rate is nevertheless reported between UHP units with isothermal decompression and early thermal reequilibration. All combinations between hot/warm/cold and fast or slow exhumations have been indeed documented (Kylander-Clark et al., 2012; McClelland and Lapen, 2013).

In order to assess the possible effects of partial melting reactions in the subduction/exhumation dynamics of continental crust during early collision, thermo-mechanical modelling has been performed using different parameterisations for melting. The Norwegian Caledonides have been chosen as a case study for moel set-up and comparison of synthetic outputs with natural data.

3. Numerical modelling

3.1 Set up and partial melting implementation

The model setup, borrowed from Duretz et al. (2012), consists of two continents separated by a 500 km wide ocean. Simulations were run with the thermomechanical code I2VIS (Gerya and Yuen, 2003, and appendix). Each lithology was characterized by a temperature-stress dependent visco-plastic rheology (rheological and flow parameters as listed in table 1). The size of the model was 4000 x 1400 km and variable grid spacing (1361 x 351 nodes) was employed to attain 1 km grid spacing in the collision area (Figure A1). We initially prescribed plate convergence rate at 5 cm/y until 500 km of convergence was achieved, then let the models be driven by buoyancy forces (e.g. slab pull). All mechanical boundary conditions were free slip. Surface and bottom temperature were kept constant, while model sides were subjected to a zero flux condition. In the simulations presented here, the initial continental crust thickness is 35 km with a linear geotherm. The oceanic domain has a 7 km thick crust with an initial thermal structure defined by a half-space cooling solution (40 Myr thermal age, 10^{-6} $m^2.s^{-1}$ diffusivity). The lithosphere asthenosphere boundary is determined by the 1573 K isotherm. Upper and lower crustal densities evolve according to the equation of state; whereas oceanic crust and mantle densities are pre-computed from phase equilibria assuming basaltic and pyrolitc compositions, respectively. The upper and lower crust are assumed to be strong (Adirondacks felsic granulite; Wilks and Carter, 1990) in order to mimic the strong Baltican shield and maximize the effect of eduction (Duretz et al, 2012a; Duretz et al, 2012b).

Surface processes (erosion and sedimentation) considered as important in subduction (Pysklywec, 2006) and continental collision (Gerya et al., 2008) have been fixed to an average value of 1 mm/yr erosion/sedimentation rate. As demonstrated in Gerya et al. (2008), erosion mainly has an impact on the late evolution of the collision wedge. In this study, we focus on the eraly stages of collision and since no quantitative value is known for the erosion rates during the Scandian collision event, a reasonable constant value has been assigned.

Partial melting is paramaterized for each lithology (table 2) and three different continental crust melting reactions were tested (Figure 1): H_2O-fluid-saturated melting, as experimentally constrained up to UHP domain (Huang and Wyllie, 1981), low-temperature undersaturated dehydration melting as determined in the plagioclase field by Castro et al. (2000) and in the jadeite field by Auzanneau et al., (2006) and eventually phengite-dehydration melting as determined by Hermann (2002), which constitutes a high T end-member of the phengite-dehydration melting curves. Estimates of second critical endpoint (Schmidt et al., 2004; Hermann and Spandler, 2007), above which the wet solidus is not defined and fluids continuously evolve from aqueous to supercitical and eventually melts, lie at 5 GPa, meaning that all reactions can be considered at least up to this pressure. Solidus and liquidus for other lithologies were implemented as T= f(P) (table 2).

In the presented model, partial melting has two important consequences. (1) In the heat equation, heat capacity is modified according to melt fraction and latent heat of melting/crystallization is taken into account. (2) Rheology is sensitive to melt fraction. At any P,T point above the solidus curve, melt fraction F is computed as $F = [T-T_{sol}(P)] / [T_{liq}(P) - T_{sol}(P)]$, with T_{sol} and T_{liq} the solidus and liquidus temperatures respectively. For F below (resp. above) RCMP, effective viscosity is the Voigt average (resp. Reuss) of the protolith viscosity in the same conditions and the general viscosity truncation value. This implementation is simple enough to be computed for any of the melting scenarios explored, and is actually a fair approximation of the qualitative strength curves deduced from experimental data (Rosenberg and Handy, 2005). Continental crust crossing its wet solidus at 3 GPa, 660 °C, reaches RCMP=0.1 at 716°C for the same pressure, and undergoes a viscosity drop from $10^{20.3}$ to $10^{17.9}$ Pa.s (Figure 2M).

In I2VIS a minimum viscosity truncation has to be set to limit the adaptative reduction of time-steps, this minimum viscosity being also attributed to the sticky air layer employed to mimic the effect of a free surface (Schmeling et al., 2008; Crameri et al., 2012). Since partial melting implementation induces high viscosity contrasts in our models, a sensitivity test has been performed to eventually use a 10^{17} Pa.s lower viscosity threshold in simulations performed to fully observe the impact of different partial melting reactions (Figure 2 A to L).

No density change has been associated to melting here since (1) different melting reactions may have opposite bulk effects on density (Clemens and Droop, 1998) and (2) the increase of subducted rocks buoyancy by partial melting enhances development of buoyant structures (e.g., Gerya et al., 2008) and thus overlaps with rheological effects, which we want to investigate in this study.

We did not take into account the extraction of melt to the surface (i.e. volcanism) since migmatites in the WGR never exceeded metatexite stage, and therefore unlikely produced large amounts of melt. No Caledonian peraluminous granite has been described so far in the WGR or in the allochthonous units overlying them. No consequent mass transfer therefore occurred due to partial melting, and migmatites can be modelled as a phase on their own without melt extraction.

3.2 Results

The sentivity tests performed to choose the lower viscosity truncation value sufficient to resolve viscosity contrasts due to partial melting show drastic differences in geometries and computation times (Figure 2). We ran our model with the H_2O-saturated melting reaction and with 10^{19}, 10^{18} and 10^{17} Pa.s viscosity truncations. In the 10^{19} Pa.s truncation case (Figure 2A to D) UHP metamorphic rocks are exhumed as a buoyant plume within the subduction channel directly to the surface, then forming a UHP nappe on top of the subducted plate (Figure 2D). In both other cases, exhumation at the plate interface is stopped at sub-crustal depth (30-40 km) and UHP rocks form a deep core (Figure 2H and L) that will be further exhumed by late orogenic processes. Viscosities in the 3 simulations allow to explain this first order difference. In the highest truncation viscosity case, the subduction interface constitutes an artifactual continuous low viscosity channel connecting UHP metamorphic rocks directly to the air. They exhume along this channel due to extreme pressure gradient. In the two other cases, low viscosity regions in the upper subduction wedge and in the UHP domain are not connected, and UHP rocks only exhume in the deeper part of the subduction interface. Considering that the differences between 10^{18} and 10^{17} Pa.s viscosity truncation cases were minor, we considered this latest value as sufficient for the comparison of the impact of different melting reactions.

Reference experiment with no crustal partial melting implemented (Figure 3A) develops a continental subduction beneath a partially hydrated mantle wedge. The geometry of the hydrated interface is continuous, even though poorly resolved in our models (rising hydrated "fingers" are only 1 mesh cell large). Contintental crust reaches maximum depth and lithostatic pressure corresponding to the UHP field (depths beyond 100 km) about 8 Myrs after the lower plate continental margin is involved in the subduction, i.e. at the same time the lower plate lithosphere starts to detach by necking at the continentocean transition (Duretz et al., 2012b). Continental crust is then relaminated in the overriding plate or exhumed along the plate interface due to lower plate rollback. The initial stages of this reference model compare both in geometry and timing with the initial stages of the subduction-eduction model proposed by Duretz and co-workers (2012a) for the Norwegian Caledonides.

Experiments with dehydration melting implemented at low or high temperature (Figure 3C and D) show very similar pattern, with slab detachment occurring about 1 Myr earlier than in the reference model. Partially molten continental crust then decouples from the lithospheric mantle, to be relaminated within the upper plate lithosphere. In the LT dehydration case exhumation of migmatites is eventually achieved at 28 Myr (ie 12 Myr after collision). In the HT dehydration case migmatites are not exhumed and remain within the lower plate.

Experiments with low temperature H_2O-fluid-saturated partial melting parametrization show a substantially different pattern (figure 3B and Figure 4). Partially molten continental crust is exhumed within the subduction interface as soon as 7 Myrs after collision initiates and acts as a low viscosity decoupling interface between the upper and lower plates (Figure 3E). They form a pointing up wedge developing into a 20 km wide crustal plume between the two converging plates. Rocks, with melt percentages up to 24 % have a high turbulence dynamics within this partially molten channel so that markers initially located away from each other in the downgoing slab eventually end out close in the partially molten domain (Figure 4C). Widening of the channel and recumbent folding of the overriding plate maintains the migmatites in lower position until they reach crustal depth (Figure 4C). Slab detachment is delayed and occurs 9 Myrs after collision. Early melting and exhumation of the subducted margin explain this difference in slab detachment timing. Early exhumation hence reduces the bulk positive buoyancy of the continental slab therefore delaying slab detachment.

Duration of residence in the eclogite field (Figure 5) has been measured for selected markers within the distal (A, C, E and G in Figure 5) and proximal continental margin (B,D,F and H in Figure 5) and range between 13.5 and 14.4 Myrs for reference non-molten model and dehydration melting models. Only the H_2O-fluid-saturated model markers yield shorter residence times for 9.7 and 10.5 Myrs for the proximal and distal marker respectively. Exhumation rates were computed in all models for the same markers in the downgoing plate. Involvement of the margin in the subduction is marked by a 3 Myr negative peak indicating burial with maximum rate between 105 and 142 mm/yr for proximal margin marker and 137 and 173 mm/yr for distal margin marker. These maximum values are actually computed over very short time intervals (80 ky). Averages for burial rates calculated over the 15-19 Ma interval yield values between 47 and 79 mm/yr, which should be compared to spontaneous convergence rate in the experiment ie 28 mm/yr average during subduction. No unequivoqual impact of partial melting on burial dynamics can be inferred from these experiments. While reference model exhibits an exhumation pulse synchronous with slab detachment at 24 Myr with maximum exhumation rate about 35 mm/yr, and average exhumation rate over the 22-32 Myr interval between 6 and 13 mm/yr, models with partial melting implemented show much more contrasted exhumation histories. LT Dehydration melting scenario (Figure 5 E and F) shows exhumation of the subducted continental margin triggered during slab detachment before partial melting occurs, with maximum exhumation rates up to 14 mm/yr. Reaching of solidus and subsequent RCMP are not correlated with an increase in exhumation rate; sensible exhumation (maximum value 49 mm/yr) is achieved later due to slab retreat. In the HT dehydration melting scenario (Figure 5 G and H), exhumation of the subducted continental margin is also triggered during slab detachment and reaches moderate exhumation rates. No exhumation is associated to melting and reaching of RCMP. In both cases average exhumation rate over the 22-32 Myr interval range between 4 and 9 mm/yr, i.e. lower values than for the reference model without melting implemented. In the H_2O-fluid-saturated melting case, exhumation rates are much higher than in the other cases. Maximum values compare with maximum burial rates (145 and 190 mm/yr for proximal and distal margin respectively), with average values over the 22-32 Myr period between 12 and 18 mm/yr. Most of exhumation is achieved over a short time interval (about 1 to 2.5 Myrs) prior to slab detachment and immediately after RCMP is reached. Exhumation is therefore synchronous to subduction, migmatites rising upward in a counterflow exhumation plume (Figure 2B) while the lower plate is still subducting.

Synthetic PT paths, directly comparable with natural data as compiled in Figure 1 were plotted for the same markers from the distal and proximal subducted passive margin (Figure 6). Markers initially equally spaced share the same prograde path in the reference model and the 3 different partial melting explored cases. PT paths for the internal margin (paths B, F and H, Figure 6) are sensibly identical for the non-melting reference case and the dehydration melting scenarios with maximum temperature about 700°C reached during decompression. Paths for external margin also compare in the reference model and the HT dehydration case, where ultra-high temperatures (UHT, > 900°C) and a high partial melting rate close to 30 % are reached during relamination in the upper lithospheric plate (circle 1 on Figure 6). PT paths for H_2O-fluid-saturated melting (C and D paths, Figure 6) coevally reach maximum pressure and temperature (not exceeding 860 and 810°C for the distal and proximal markers respectively) and then undergo exhumation via isothermal or slightly cooling trajectories. RCMP (ie 0.1

melt fraction rate is reached close to peak and maximum melt fractions reached are about 20 %. Chaotic portions of the path (as along path D at 2.6 GPa, Figure 6) betray mixing within the partially molten plume. PT path for the external margin in the LT dehydration case shows an intermediate shape (path E, Figure 6), with maximum P reached in the non-molten domain, and a change in PT path slope when RCMP value is reached, with a nearly isothermal decompression at temperature between 910 and 850°C along the 20% melt fraction curve. Apart from external margin markers in the reference and HT dehydration models (A and G paths), all markers end out noteworthily in a common PT domain around 2 GPa and 700°C (circle 2 on Figure 6).

4. Discussion

Our models show that low temperature (in the 600-700°C temperature range) melting, i.e. in the presence of free fluid, drastically modifies collision wedge dynamics with the development of a low viscosity buoyancy-driven exhumation plume early in the collision history. Exhumation of UHP partially molten continental rocks is facilitated by the rheological weakening due to partial melting and PT paths of these units share a high rate isothermal exhumation stage just after peak pressure and temperature are coevally reached. In order to realistically resolve this process in our numerical models, a low viscosity truncation is needed, not higher than 10^{18} Pa.s. The exhumation dynamics produced is considered as more realisitic than the one stage nappe-like exhumation obtained for high viscosity truncation (Figure 2 A to D) for 1- it reproduces the observed tectonostratigraphy in the WGR: UHP rocks form domes below HP domains rather than nappes on top of lower grade rocks, and 2- it decouples deep and shallow orogenic exhumation dynamics and explains the two stage PT paths documented in the WGR and in most of the UHP domains worldwide.

Validation of the presented models can be achieved through the comparison of melt fractions in the migmatites, residence time intervals in the eclogites field, synthetic burial and exhumation rates and eventually PT paths with natural data from the Norwegian Caledonides used as a case study.

In the WGR, melt fractions observed in the migmatites are not higher than 30%, resulting in metatexite textures only. Even though these textures do not evidence the absence of melt mobility, they actually imply that this mobility remained local, and that no substantial melt extraction occurred. The absence of Caledonian leucogranites can confirm this assertion. Models computed therefore must also comply with this low melt mobility hypothesis. Melt fractions achieved by markers within the migmatitic UHP unit (Figure 4 and 6) reach maximum values close to 30%. They reach 24 % for the migmatite plume in the H_2O-fluid-saturated melting model, and 32% in the HT dehydration partial melting model, where migmatites are relaminated in the upper plate. The condition of low melt fraction is therefore respected, and the consideration of migmatites as a rheological phase on their own is valid here. Extraction could actually be relevantly considered in the high melt fraction relaminated material in the HT dehydration model. In the case of H_2O-fluid-saturated melting, the 20 % melt fraction reached by the migmatites at 850°C and 3 GPa along their retrograde path (Figure 6) imply 2 wt % H_2O initially present according to recent experimental data compilations (Mann and Schmidt, 2015). Even if no definitive numbers are assigned to fluid fluxes in the deep part of orogens, dehydration reactions in the mantle are prone to produce fluids in the same proportions. These values are therefore not out of range.

Residence times in the garnet-crystallization field have been estimated in the WGR through paired Lu-Hf and Sm-Nd dating on eclogites (Kylander-Clark et al., 2009 and references therein). These values can be considered as minimum equivalents of the residence time in the eclogite facies as computed for our markers. The four meaningful age pairs in the 390-420 Ma range documented in the WGR give minimum residence durations of 17 to 9 Myrs for eclogites sampled out of the UHP domains, and 6 Myrs for the UHP eclogite analyzed in the Sorøyane UHP domain (Kylander-Clark et al., 2009). Our models give comparable values for residence in the eclogite field (9.7 to 14.4 Myrs). The coincidence between the shorter residence time computed for the H_2O-fluid-saturated melting model and with the shorter Lu-Hf/Sm-Nd age difference measured in a migmatite-hosted UHP eclogite is to be noted. Nevertheless uncertainties on the age differences being the same order of magnitude as their values, this fitting may be not conclusive.

Spontaneous burial rate during continental subduction (47 to 79 mm/a) also lay within the order of magnitude of convergence rate admitted for Laurentia-Baltica convergence at the onset of the Scandian collision (Torsvik et al., 1996). Instantaneous exhumation rates derived from the model (Figure 5) have absolute values 1 order of magnitude higher than ever recorded in high-pressure rocks. The highest values are computed on very short time steps (down to 32 kyrs) while significant exhumation rates can only be confidently assessed from natural data over time intervals larger than uncertainties on radiochronological data, i.e. not less than a few Myrs. Average values from numerical models yield more realistic estimates. The 4 to 18 mm/yr exhumation rates computed for external to internal margin markers in the different models compare in order of magnitude with the range of values deduced from natural data in the NWGR (100 km exhumation over 5 Myrs, ie 20 mm/yr, Hacker et al., 2007). The models also show that long residence time in the eclogites field do not imply slow subduction or slow exhumation as argued by some authors in the WGR on the basis of scatter of cystallization ages for eclogites (Kylander-Clark et al., 2008; Kylander-Clark et al., 2009). H2O-fluid-saturated melting case yields the fastest exhumations with average rates over 10 mm/yr (12 to 18 mm/yr for external to internal margin) for the very first stages of exhumation. In this prospect, it is worth comparing synthetic data with exhumation timing and rates in SWGR, where UHP eclogites are exhumed without significant melting, and NWGR where UHP eclogites are closely associated to migmatites. SWGR have equilibrated at UHP at 410-400 (Kylander-Clark and Hacker, 2014), while NWGR UHP eclogites reached peak at 415-420 and reeequilibrated at HP at 400 Ma (Terry et al., 2000). Calculation of exhumation rates (Labrousse et al., 2004) for the different UHP domains yield slightly lower values (2.7 to 2.3 mm/a) for SWGR than for NWGR (8.1 mm/a) at least for the initial exhumation stages. Although these 10 to 5 Myrs differences in timing are within radiochronology uncertainties, it seems therefore that SWGR exhumed later and slower than NWGR. Our model could actually fit these data considering the proximal marker in our non-molten simulation as representative for SWGR UHP domain and the distal marker of our H_2O-fluid-saturated melting model as representative for NWGR UHP domain. This would imply that NWGR initially had a more distal position than SWGR, which is possible but not corroborated by any geological data.

Temperature ranges reached by UHP rocks in the models are in good agreement with natural values and actually constitute a better discrimination criterion between models. Only H_2O-fluid-saturated melting scenario produces UHP rocks with peak conditions and subsequent decompression in the documented 750-850°C range (as in Hacker al., 2007 and reference therein). Proximal marker exhumed in the non-molten model

(Figure 5B) reaches 740°C during retrogression which is slightly higher than what was recorded in the non-molten SWGR (Labrousse et al., 2004; Kylander-Clark and Hacker; 2014). A marker intentionaly taken further inside the margin could actually fit this value, so that this inadequation is not critical. Other melting scenarios produce higher temperature trajectories with UHT reached during decompression, while no index of such extreme crystallization conditions has been recorded so far in the WGR. Peak pressures reached by the chosen markers in the models (between 3.7 and 5.2 GPa, Figure 5) fall between the usually documented pressures in the NWGR (maximum 3.8 GPa in Hacker, 2007) from thermo-barometry on phengite-bearing eclogites mainly and higher values (5.5 to 6.5 GPa) locally computed from garnet peridotites and websterites included within the NWGR (Vrijmoed et al., 2006, van Roermund et al., 2009). The width of the exhumation plume developing in the H_2O-fluid-saturated melting case (~ 20 km on Figure 3B) is slightly larger than the minimum width of 10-15 km alleged for the average WGR UHP "unit" based on heat diffusion considerations (Hacker et al., 2007). While the latest stages of exhumation of the WGR UHP rocks are associated to crustal dynamics beyond the scope of the present study, their initial exhumation could actually be due to decoupling and upward rising of a partially molten crustal unit as imaged in the H_2O-fluid-saturated model computed here. The structural position of the WGR migmatite-bearing UHP domains depicted as diffuse boundary domes cropping out beneath the lesser metamorphosed Baltican crust (Labrousse et al., 2002; 2004; Hacker et al., 2007) is also reproduced by our model (Figure 4C). The lower scale aspect of the WGR migmatite-bearing UHP province, i.e. meter to hectometer mafic and ultramafic bodies included in a highly strained migmatite matrix could actually be inherited from high rate mixing within such a migmatitic plume (Figure 4B). The km-size areas described in the WGR as subducted and exhumed without substantial deformation

(Hacker et al., 2010) are not reproduced in our model, where the whole migmatite plume is affected by intense mixing. Differences in protoliths permeability and initial chemistry argued for explaining their differential reactivities and strength in UHP conditions are not implemented in our model, and small scale strain pattern within the migmatitic exhumed unit is probably not relevant. The continental crust modeled here is indeed homogeneous and reacts instantly and completely to pressure-temperature changes.

The intersection of synthetic PT paths at 2GPa, 700°C (circle 2 on Figure 6) is similar to a common retrogression domain noticed in the natural data from the different UHP rocks in the WGR but at slightly lower conditions (1GPa, 600°C, Labrousse et al., 2004). Both actually have the same geodynamic significance. These PT domains represent the transition between exhumation in the mantle (at higher pressures) and within the crust (at lower pressure). In both cases they coincide with a decrease in exhumation rate, possibly explaining why these conditions are actually recorded by recrystallization in the metamorphic rocks. The comparison of our models outputs with independent data from the natural case, which we chose to define their set-up, show that these data are best reproduced by the H_2O-fluid-saturated melting model for the NWGR. The differences between NWGR and SWGR exhumation rates and timing are also reproduced, considering that proximal markers in the no-melting model are representative of SWGR.

Our H_2O-fluid-saturated partial melting model is also consistent with previous models dedicated to exhumation of UHP continental rocks after continental subduction (Warren et al., 2008; Gerya et al., 2008, Sizova et al., 2012). Our set-up would range in the high initial viscosity for the continental margin and high weakening factor, meant to model partial melting reactions among others. Our model yields exhumation of rocks from comparable PT conditions and with a comparable geometry. Our partially molten plume is an equivalent of the weak plume exhuming in type III models in Warren et al. (2008). PT paths however differ; models encompassing weakening only due to strain (Warren et al, 2008) and no partial melting parameterisation fail at reproducing initial isothermal decompression in PT paths.

Relamination of partially molten rocks in the upper plate as exhibited by the HT dehydration model (Figure 2D, path G on Figure 6) even if not relevant for the Norwegian Caledonides case has already been suggested as a mechanism for the development of felsic continental lower crust (Hacker, 2011). Difference between our models and conceptual model for relamination is the depth of intercalation of lower plate material (subcrustal in Hacker et al., 2011 vs intra-lithosphere in our models). Rise of crustal material in our models is not only controlled by the density contrast but also by the strength of the surrounding mantle (i.e. Stokes' law). The high melt fraction achieved by this material would actually require the computation of melt extraction to better resolve this process.

A possible link between partial melting of the continental crust in a convergent setting and lithospheric delamination or slab detachment has already been proposed. Thermal relaxation of the collision zone and advection of asthenospheric mantle are mentionned as possible causes for anatexis. Numerical models (Faccenda et al., 2008) show that high radiogenic heat continental crust promotes slab detachment by heating and subsequent weakening of the collisional wedge. No study so far pointed at the possible role of crustal melting on slab detachment. The present study shows that whatever the partial melting parameterisation implemented if any, slab detachment occurs merely at the same time (i.e. ± 1 Myr in the collision history). Partial melting of the fertile upper plate, concerning the upper 10 to 20 km of the lithospheric pile, has no noteworthy impact on slab detachment dynamics. Even if not at the same scale, slab detachment and partial melting rather appear as two independent mechanisms prone to limit continental subduction and trigger the exhumation of UHP continental rocks.

The compilation of PT paths for UHP continental units or domains worldwide systematically show peak conditions close to one of the acknowledged reaction curve for anatexis and an initial exhumation stage with slightly isothermal decompression (Figure 1). The models presented here were designed to reproduce the Caledonian orogen, which appears to be a low temperature end-member in terms of thermal state (Labrousse et al., 2010), but some of our conclusions may have broader implications. The shape of PT paths for other UHP migmatite-bearing units worldwide may actually sign their melting at peak conditions. It is indeed expected and visible in our models that exhuming UHP units induce an upward curvature of isotherms during decompression, due to 1) high exhumation rates relative to heat diffusion, and 2) heating of the surrounding rocks by latent heat dissipation during recrystallization. The reason why the relevant reaction changes with orogen must reside in the initial chemical composition of the subducted continental crust. H_2O, and K_2O contents at first order, controlling the amount of mica available for melting (Massonne, 2009). The LT dehydration model with maximum temperatures about 900°C reached by the subducted margin, initial exhumation triggered by slab detachment and fast exhumation lately facilitated by retrograde partial melting show striking similarities with the conceptual model proposed for the Kokchetav UHP massif (Hermann et al., 2001). The peak PT conditions coinciding with HT dehydration curve (Figure 1) could also correspond to reaching of high RCMP isopleth related to LT dehydration solidus. Proper modelling with set-up inspired from Kokchetav would be necessary to further investigate this hypothesis. Also our models were not designed to test the impact of several melting reactions occuring throughout the prograde stages. In reality, it might be possible that polybaric melting results in a finite product marked by dehydration melting reactions, although the very first increments of melting were associated to H_2O-fluid-saturated partial melting.

Conclusion

Even though H_2O-fluid-saturated melting is often considered as a second-order process in terms of magma production, the present study tends to show a possible rheological first order impact of this reaction in the subduction-collision dynamics, in the Norwegian Caledonides case study at least. H_2O-fluid-saturated partial melting as parameterized here, and with all other parameters kept equal, actually limits continental subduction and facilitates upward flow of partially molten rocks early in the collision history, i.e. prior to any slab detachment. Migmatites develop into an exhuming plume, which acts as a decoupling layer separating the two converging plates. In this buoyancy driven plume, UHP migmatites exhume at rates comparable to their burial rate. Synthetic pressure-temperature-time paths produced are very similar to natural data from the Caledonides, with high initial exhumation rates and isothermal decompression following coevally reached peak pressure and temperature. The proposed triggering effect of H_2O-fluid-saturated melting on exhumation from field and experimental perspectives (Labrousse et al., 2011, Ganzhorn et al., 2014) is shown to be also thermo-mechanically sound. Other possible melting reactions for continental crust, i.e. dehydration melting, do not drastically change subduction-collision dynamics. Slab detachment remains the first order process limiting continental subduction in these cases. They nevertheless could be key reactions in explaining the exhumation of warmer migmatite-bearing UHP units in collisional orogens, which also show high rate initial isothermal decompression and peak PT conditions close to higher temperature solidus curves for continental material.

Acknowledgements

The present work was initiated while T. Duretz was a post-doc at ISTEP, UPMC. The ANR Project ON:LAP and P. Agard should be thanked for that. It is part of ERC Rheolith project (PI L. Jolivet, E. Burov). An anonymous reviewer and Bradley Hacker greatly improved the present manuscript by their thorough and constructive reviews. It also benefitted from discussions with T. B. Andersen. The authors would like to thank all these colleagues.

Appendix : Numerical methods and set-up

The presented numerical simulations were carried out using the code I2VIS (Gerya and Yuen, 2003). The Stokes equations, the incompressible mass conservation equation, and the energy conservation equation, take the form of:

$$\frac{\partial \tau_{ij}}{\partial x_j} - \frac{\partial P}{\partial x_i} = \rho g_i$$

$$\frac{\partial v_i}{\partial x_i} = 0$$

$$\frac{\partial}{\partial x_i}\left(k \frac{\partial T}{\partial x_i}\right) = \rho C_p \frac{DT}{Dt} - H$$

where τ_{ij} is the deviatoric stress tensor, P is the pressure, ρ is the density, g_i is the gravitational acceleration, v_i is the velocity vector, k is the temperature-dependent thermal conductivity (table 1), T is the temperature, C_p is the heat capacity, and H corresponds to heat sources (radioactive heat production, shear heating, adiabatic heating, and latent heat). These equations are solved with the finite difference/marker-in-cell method (see Gerya, 2010; Duretz et al, 2011 for technical aspects). The diffusive fluxes and production terms are discretized on a 2D Eulerian staggered grid, whereas the advective fluxes are treated on Lagrangian particles.

The rheology is visco-plastic taking into account contributions of diffusion-dislocation creep, exponential creep (mantle lithosphere only), and Mohr-Coulomb rheology. Viscosities corresponding to each flow mechanism are computed as follows:

$$\eta_{\mathrm{viscous}} = \eta_0^{\frac{1}{n}} \dot{\varepsilon}_{II}^{\frac{1-n}{2n}} e^{\left(\frac{E_A + PV_A}{nRT}\right)}$$

$$\eta_{\mathrm{exponential}} = \left\{ 2A_{\mathrm{Peierls}}\, e^{\left(\frac{E_A + PV_A}{RT}\right)} e^{\left(1-\left(\frac{\tau_{II}}{\sigma_{\mathrm{Peierls}}}\right)^k\right)^q} \right\}^{-1}$$

$$\eta_{\mathrm{Mohr-Coulomb}} = \frac{C + P \sin\varphi}{2\dot{\varepsilon}_{II}}$$

The reference viscosities (η_0), stress exponents (n), activation energies (E_A), activation volumes (V_A), the cohesion (C), and the internal friction angle (φ) are listed in table 1 and R is the gas constant. The parameters of exponential creep are taken as $A_{\mathrm{Peierls}} = 10^{7.8}10^{-12}$ Pa-2s-1 and $\sigma_{\mathrm{Peierls}} = 9.1$ GPa. The second deviatoric stress (τ_{II}) and strain rate ($\dot{\varepsilon}_{II}$) invariants are expressed as

$$\tau_{II} = \sqrt{\tau_{ij}\tau_{ij}}$$

and

$$\dot{\varepsilon}_{II} = \sqrt{\dot{\varepsilon}_{ij}\dot{\varepsilon}_{ij}}$$

The flow rule that produces to the minimum viscosity is defined as the dominant deformation mechanism:

$$\eta_{eff} = \min \left(\eta_{viscous}, \eta_{exponential}, \eta_{Mohr-Coulomb}\right)$$

and the stress-strain rate relationship is subsequently expressed as:

$$\tau_{ij} = 2\,\eta_{eff}\,\dot{\varepsilon}_{ij}\ ,$$

where η_{eff} is the effective viscosity, and $\dot{\varepsilon}_{ij}$ corresponds to the strain rate tensor. The rheological impact of melting is described in the main text.

The density of mafic (gabbroic composition) and ultramafic (pyrolitic composition) material phases is temperature and pressure dependent. Densities are evaluated at each timestep from look-up tables that are precomputed via Gibbs energy minimization in the CaO-FeO-MgO-Al_2O_3-SiO_2 system (Gerya et al, 2004). The density of felsic materials obey the following equation of state:

$$\rho = \rho_0 \left[1 - \alpha(T - 298.5)\left(1 + \beta(10^{-8}P - 10^{-3})\right)\right].$$

The reference density (ρ_0) of the upper and lower continental crusts are 2700 kg/m3 and 2800 kg/m3 respectively. The isothermal compressibility is set to 0.5 10^{-3} kbar-1 and the thermal conductivity is set to 1.5 10^{-5} K-1.

The free surface is approximated by a sticky air approach (Crameri et al, 2012). The air layer is 20 km thick and its viscosity is set to the lower viscosity cut-off (see figure 2).

Surface processes are modeled using a gross-scale erosion sedimentation law (Gerya, 2010) and the topography (h) evolves according to:

$$\frac{\partial \mathrm{h}}{\partial \mathrm{t}} = \mathrm{v}_{\mathrm{y}}^{\mathrm{h}} - \mathrm{v}_{\mathrm{x}}^{\mathrm{h}} \frac{\partial \mathrm{h}}{\partial \mathrm{x}} - \dot{\mathrm{e}} + \dot{\mathrm{s}},$$

where $\mathrm{v}_{\mathrm{x}}^{\mathrm{h}}$ and $\mathrm{v}_{\mathrm{y}}^{\mathrm{h}}$ corresponds to the velocity components of the model's surface, $\dot{\mathrm{e}}$ and $\dot{\mathrm{s}}$ are prescribed erosion and sedimentation rates (0.1 mm/y).

Table & Figure captions

Table 1: Thermal and mechanical parameters employed in the numerical simulations: k is the temperature dependent thermal conductivity expressed as a function T, absolute temperature in K, Hr is the radiogenic heat production, Cp is the specific heat capacity, sin(f) is the friction coefficient, C is the cohesion, h_0 is the reference viscosity, n is the stress exponent, E_a is the activation energy, and V_a is the activation volume. sediments and upper oceanic crust (UOC) modeled as wet quartzite (1, Ranalli and Murphy, 1987), upper and lower continental crust (UCC, LCC) modeled as felsic granulite (2, Wilks and Carter, 1990), lower oceanic crust (LOC) modeled as anorthosite (3, Ranalli and Murphy, 1987), dry mantle (Dry M.) modeled as dry dunite (4, Chopra and Paterson, 1984), serpentinized and wet mantle modeled as wet olivine (5, Ranalli, 1995).

Table 2 : Various solidus employed in the simulations. H_2O-fluid-saturated, Low T dehydration and high T dehydration were used to simulate sediment and upper continental crust melting. Wet basalt melting was employed for mafic lithologies (lower continental crust, oceanic crust). Dry and Wet mantle solidus were used for melting of dry and hydrated ultramafic lithologies.

Figure 1: PT-paths for UHP metamorphic units and solidus curves used in numerical models for the continental crust. H_2O-fluid-saturated solidus from (Huang and Wyllie, 1981), low temperature dehydration-melting solidus from (Auzanneau et al., 2006) and (Schmidt et al., 2004) and high temperature dehydration melting as experimentally defined by Hermann et al. (2002). PT-paths for South and North Western Gneiss Region (SWGR, NWGR Labrousse, 2004), North East Greenland Eclogite Province (NEGEP, McClelland and Lapen, 2013), South Dabie Chan (SDC) and Central Dabie Dome (CDD) compiled in Faure et al. (2003), Sulu Orogen (SO, Chen et al., 2013), Kokchetav

massif (KM, Hermann et al., 2001), Erzgebirge (ERZ, Massonne, 2003)),Dora Maira (DM, Chopin and Schertl, 1999) and Lago di Cignana (LdC, Reinecke, 1998). Coesite and eclogites stability field as in (Liou et al., 2004).

Figure 2: Effect of general viscosity truncation value used for computation. A to D : viscosity truncation 10^{19} Pa.s, E to H : viscosity truncation 10^{18} Pa.s and I to L : viscosity truncation 10^{17} Pa.s. M: viscosity drop implementation due to continental crust partial melting in the designed model (curve drawn for H_2O-fluid-saturated melting at P = 3 GPa, strain rate = 10^{-15} s^{-1}). Phase colors legend precised in Figure 3.

Figure 3: Model results 8 Ma after initiation of collision. A, without any melting effect implemented, B, with H_2O-fluid-saturated melting, C with low temperature dehydration melting and D with high temperature dehydration melting. E: viscosity field for H_2O-fluid-saturated melting experiment. u/l..c.c./o. upper/lower continental/oceanic crust, serp./hydr. l.m. serpentinized/hydrated lithospheric mantle, a. m. asthenospheric mantle. Numbers for rheologies 1 to 5 refer to table 1, 6 & 7 computed according to table 2 equations.

Figure 4: Time evolution of H_2O-fluid-saturated partial melting model. The color code for phases is similar to figure 3. Isotherms in degree Celsius. Melt fraction is color-coded for partially molten crust in insets. Only 800°C isotherm (dashed line) is reported there. Arrows on sketches indicate shear senses and flow directions within the subduction zone.

Figure 5: Vertical velocity-time curves for 2 markers within the subducted continental margin (circles and squares refer respectively to circle and square on inset I). Change from dashed to continuous line represents solidus crossing, simple black arrows show

when RCMP is reached. Grey rectangles show residence time interval in the eclogites field as delimited in Figure 5. Arrow endings for A and G mean these markers did not exhume from eclogites field. White double arrows indicate slab detachment timings for each experiment along the paired advection-time curves. l.m. lithospheric mantle, c.c. continental crust, o.c. oceanic crust.

Figure 6: Pressure-temperature paths for markers initially located in the lower plate margin (inset I Figure 4) and different melting reactions implemented. A to H refer to curves in Figure 5. Iso-melt fraction curves are drawn for each experimentPrograde paths, superposing each other have been cut for readability purposes. Coesite and eclogites stability field as in Liou et al. (2004).

Figure A1: Initial model configuration. The different colors correspond to various material phases (see legend figure 3) and the red square indicates the areas of high numerical resolution. The initial plate velocity is imposed within the plates (black arrows). The continental plates subsequently decouple from the lateral box sides during convergence. The isotherms (white lines) are plotted for each 400° C increment.

References

Auzanneau, E., Vielzeuf, D., and Schmidt, M.W., 2006, Experimental evidence of decompression melting during exhumation of subducted continental crust: Contributions to Mineralogy and Petrology, v. 152, no. 2, p. 125–148, doi: 10.1007/s00410-006-0104-5.

Blanckenburg, von, F., and Davies, J.H., 2010, Slab breakoff: A model for syncollisional magmatism and tectonics in the Alps: Tectonics, v. 14, no. 1, p. 120–131, doi: 10.1029/94TC02051.

Castro, A., Corretgé, L.G., El-Biad, M., El-Hmidi, H., Fernandez, C., and Douce, A.E.P., 2000, Experimental Constraints on Hercynian Anatexis in the Iberian Massif, Spain: Journal of Petrology, v. 41, no. 10, p. 1471–1488, doi: 10.1093/petrology/41.10.1471.

Chen, Y.X., Zheng, Y.F., and Hu, Z., 2013, Synexhumation anatexis of ultrahigh-pressure metamorphic rocks: Petrological evidence from granitic gneiss in the Sulu orogen:, v. 156-159, p. 69–96, doi: 10.1016/j.lithos.2012.10.008.

Chopin, C., and Schertl, H.-P., 1999, The UHP Unit in the Dora-Maira Massif, Western Alps: International Geology Review, v. 41, no. 9, p. 765–780, doi: 10.1080/00206819909465168.

Chopra, P.N., and Paterson, M.S., 1984, The role of water in the deformation of dunite: Journal of Geophysical Research, v. 89, no. B9, p. 7861–7876, doi: 10.1029/JB089iB09p07861.

Clemens, J.D., and Droop, G., 1998, Fluids,paths and the fates of anatectic melts in the Earth's crust: Lithos, v. 44, no. 1-2, p. 21–36, doi: 10.1016/S0024-4937(98)00020-6.

Crameri, F., Schmeling, H., Golabek, G.J., Duretz, T., Orendt, R., Buiter, S.J.H., May, D.A., Kaus, B.J.P., Gerya, T.V., and Tackley, P.J., 2012, A comparison of numerical surface topography calculations in geodynamic modelling: an evaluation of the "sticky air" method: Geophysical Journal International, v. 189, no. 1, p. 38–54, doi: 10.1111/j.1365-246X.2012.05388.x.

Duretz, T, D. A. May, T. V. Gerya and P. J. Tackley, 2011. Discretization errors and free surface stabilization in the finite difference and marker-in-cell method for applied geodynamics: A numerical study, Geochemistry, Geophysics, Geosystems, Vol. 12, Q07004

Duretz, T., Gerya, T.V., Kaus, B.J.P., and Andersen, T.B., 2012a, Thermomechanical modeling of slab eduction: Journal of Geophysical Research, v. 117, no. B8, p. B08411, doi: 10.1029/2012JB009137.

Duretz, T., Schmalholz, S.M., and Gerya, T.V., 2012b, Dynamics of slab detachment: Geochemistry,, doi: 10.1029/2011GC004024.

Faccenda, M., Gerya, T.V., and Chakraborty, S., 2008, Styles of post-subduction collisional orogeny: Influence of convergence velocity, crustal rheology and radiogenic heat production: Lthos, v. 103, no. 1-2, p. 257–287, doi: 10.1016/j.lithos.2007.09.009.

Faure, M., Lin, W., Schärer, U., Shu, L., Sun, Y., and Arnaud, N., 2003, Continental subduction and exhumation of UHP rocks. Structural and geochronological insights from the Dabieshan (East China): Lithos, v. 70, no. 3-4, p. 213–241, doi: 10.1016/S0024-4937(03)00100-2.

Ferrero, S., Wunder, B., Walczak, K., O'Brien, P.J., and Ziemann, M.A., 2015, Preserved near ultrahigh-pressure melt from continental crust subducted to mantle depths: Geology,, doi: 10.1130/G36534.1.

Fumagalli, P., Poli, S., Fischer, J., Merlini, M., and Gemmi, M., 2014, The high-pressure stability of chlorite and other hydrates in subduction mélanges: experiments in the system Cr2O3–MgO–Al2O3–SiO2–H2O: Contributions to Mineralogy and Petrology, v. 167, no. 2, p. 979–16, doi: 10.1007/s00410-014-0979-5.

Ganzhorn, A.C., Labrousse, L., Prouteau, G., Leroy, C., Vrijmoed, J.C., Andersen, T.B., and Arbaret, L., 2014, Structural, petrological and chemical analysis of syn-kinematic migmatites: insights from the Western Gneiss Region, Norway: Journal of Metamorphic Geology,,doi: 10.1111/jmg.12084.

Gerya, T.V., 2010. Introduction to Numerical Geodynamic Modelling. Cambridge University Press.

Gerya, T.V., and Yuen, D.A., 2003, Characteristics-based marker-in-cell method with conservative finite-differences schemes for modeling geological flows with strongly variable transport properties: Physics of the Earth and Planetary Interiors, v. 140, no. 4, p. 293–318, doi: 10.1016/j.pepi.2003.09.006.

Gerya, T.V., Yuen, D.A., Maresch, W., 2004. Thermomechanical modelling of slab detachment. Earth and Planetary Science Letters 226 (1–2), p. 101–116.

Gerya, T.V., Perchuk, L.L., and Burg, J.P., 2008, Transient hot channels: Perpetrating and regurgitating ultrahigh-pressure, high-temperature crust–mantle associations in collision belts: Lithos, v. 103, no. 1-2, p. 236–256, doi: 10.1016/j.lithos.2007.09.017.

Gilotti, J.A., and McClelland, W.C., 2007, Characteristics of, and a Tectonic Model for, Ultrahigh-Pressure Metamorphism in the Overriding Plate of the Caledonian Orogen: dx.doi.org, v. 49, no. 9, p. 777–797, doi: 10.2747/0020-6814.49.9.777.

Gordon, S.M., Whitney, D.L., Teyssier, C., and Fossen, H., 2013, U–Pb dates and trace-element geochemistry of zircon from migmatite, Western Gneiss Region, Norway: Significance for history of partial melting in continental subduction: Lithos, v. 170-171, p. 35–53, doi: 10.1016/j.lithos.2013.02.003.

Hacker, B., 2007, Ascent of the ultrahigh-pressure Western Gneiss Region, Norway, *in* Special Paper 419: Convergent Margin Terranes and Associated Regions: A Tribute to W.G. Ernst, Geological Society of America, p. 171–184.

Hacker, B.R., Kelemen, P.B., and Behn, M.D., 2011, Differentiation of the continental crust by relamination: Earth and Planetary Science Letters, v. 307, no. 3-4, p. 501–516, doi: 10.1016/j.epsl.2011.05.024.

Hacker, B.R., Andersen, T.B., Johnston, S., Kylander-Clark, A.R.C., Peterman, E.M., Walsh, E.O., and Young, D., 2010, High-temperature deformation during continental-margin subduction & exhumation: The ultrahigh-pressure Western Gneiss Region of Norway: Tectonophysics, v. 480, no. 1-4, p. 149–171, doi: 10.1016/j.tecto.2009.08.012.

Hacker, B.R., Ratschbacher, L., Webb, L., Ireland, T., Walker, D., and Shuwen, D., 1998, U/Pb zircon ages constrain the architecture of the ultrahigh-pressure Qinling–Dabie Orogen, China: Earth and Planetary Science Letters, v. 161, no. 1-4, p. 215–230, doi: 10.1016/S0012-821X(98)00152-6.

Hacker, B.R., Ratschbacher, L., Webb, L., McWilliams, M.O., Ireland, T., Calvert, A., Dong, S., Wenk, H.R., and Chateigner, D., 2000, Exhumation of ultrahigh-pressure continental crust in east central China: Late Triassic-Early Jurassic tectonic unroofing: Journal of Geophysical Research: Solid Earth (1978–2012), v. 105, no. B6, p. 13339–13364, doi: 10.1029/2000JB900039.

Hermann, J., and Spandler, C.J., 2007, Sediment Melts at Sub-arc Depths: an Experimental Study: Journal of Petrology, v. 49, no. 4, p. 717–740, doi: 10.1093/petrology/egm073.

Hermann, J., Rubatto, D., Korsakov, A., and Shatsky, V.S., 2001, Multiple zircon growth during fast exhumation of diamondiferous, deeply subducted continental crust (Kokchetav Massif, Kazakhstan): Contributions to Mineralogy and Petrology, v. 141, no. 1, p. 66–82, doi: 10.1007/s004100000218.

Hermann, J., Spandler, C., Hack A., and Korsakov, A., 2006, Aqueous fluids and hydrous melts in high-pressure and ultra-high pressure rocks: Implications for element transfer in subduction zones: Lithos, v. 92, no. 3-4, p. 399–417, doi: 10.1016/j.lithos.2006.03.055.

Hermann, J.X.R., 2002, Experimental constraints on phase relations in subducted continental crust: Contributions to Mineralogy and Petrology, v. 143, no. 2, p. 219–235, doi: 10.1007/s00410-001-0336-3.

Huang, W.L., and Wyllie, P.J., 1981, Phase relationships of S-type granite with H2O to 35 kbar: Muscovite granite from Harney Peak, South Dakota: Journal of Geophysical Research: Solid Earth, v. 86, no. B11, p. 10515–10529, doi: 10.1029/JB086iB11p10515.

Kylander-Clark, A., and Hacker, B.R., 2014, Age and significance of felsic dikes from the UHP western gneiss region: Tectonics,, doi: 10.1002/(ISSN)1944-9194.

Kylander-Clark, A.R.C., Hacker, B.R., and Mattinson, C.G., 2012, Size and exhumation rate of ultrahigh-pressure terranes linked to orogenic stage: Earth and Planetary Science Letters, v. 321-322, p. 115–120, doi: 10.1016/j.epsl.2011.12.036.

Kylander-Clark, A.R.C., Hacker, B.R., and Mattinson, J.M., 2008, Slow exhumation of UHP terranes: Titanite and rutile ages of the Western Gneiss Region, Norway: Earth and

Planetary Science Letters, v. 272, no. 3-4, p. 531–540, doi: 10.1016/j.epsl.2008.05.019.

Kylander-Clark, A.R.C., Hacker, B.R., Johnson, C.M., Beard, B.L., and Mahlen, N.J., 2009, Slow subduction of a thick ultrahigh-pressure terrane: Tectonics, v. 28, no. 2,, doi: 10.1029/2007TC002251.

Labrousse, L., Hetényi, G., Raimbourg, H., Jolivet, L., and Andersen, T.B., 2010, Initiation of crustal-scale thrusts triggered by metamorphic reactions at depth: Insights from a comparison between the Himalayas and Scandinavian Caledonides: Tectonics, v. 29, no. 5, doi: 10.1029/2009TC002602.

Labrousse, L., Jolivet, L., Agard, P., Hébert, R., and Andersen, T.B., 2002, Crustal-scale boudinage and migmatization of gneiss during their exhumation in the UHP Province of Western Norway: Terra Nova, v. 14, no. 4, p. 263–270, doi: 10.1046/j.1365-3121.2002.00422.x.

Labrousse, L., Jolivet, L., Andersen, T.B., Agard, P., Hébert, R., Maluski, H., and Schärer, U., 2004, Pressure-temperature-time deformation history of the exhumation of ultra-high pressure rocks in the Western Gneiss Region, Norway, *in* Whitney, D.L., Teyssier, C., and Siddoway, C.S. eds., Geological Society of America, p. 155–183.

Labrousse, L., Prouteau, G., and Ganzhorn, A.C., 2011, Continental exhumation triggered by partial melting at ultrahigh pressure: Geology, v. 39, no. 12, p. 1171–1174, doi: 10.1130/G32316.1.

Lang, H.M., and Gilotti, J.A., 2007, Partial melting of metapelites at ultrahigh-pressure conditions, Greenland Caledonides: Journal of Metamorphic Geology, v. 25, no. 2, p. 129–147, doi: 10.1111/j.1525-1314.2006.00687.x.

Liou, J.G., Tsujimori, T., and Zhang, R.Y., 2004, Global UHP metamorphism and continental subduction/collision: the Himalayan model: International Geology …, v. 46, no. 1, p. 1–27, doi: 10.2747/0020-6814.46.1.1.

Liu, F.L., Robinson, P.T., and Liu, P.H., 2012, Multiple partial melting events in the Sulu UHP terrane: zircon U-Pb dating of granitic leucosomes within amphibolite and gneiss: Journal of Metamorphic Geology, v. 30, no. 8, p. 887–906, doi: 10.1111/j.1525-1314.2012.01005.x.

Mann, U., and Schmidt, M.W., 2015, Melting of Pelitic Sediments at Subarc Depths: 1. Flux vs. Fluid-Absent Melting and a Parameterization of Melt Productivity: Chemical Geology,, p. 1–60, doi: 10.1016/j.chemgeo.2015.02.032.

Massonne, H.-J., 2003, A comparison of the evolution of diamondiferous quartz-rich rocks from the Saxonian Erzgebirge and the Kokchetav Massif: are so-called diamondiferous gneisses magmatic rocks?: Earth and Planetary Science Letters, v. 216, no. 3, p. 347–364, doi: 10.1016/S0012-821X(03)00512-0.

McClelland, W.C., and Lapen, T.J., 2013, Linking Time to the Pressure-Temperature Path for Ultrahigh-Pressure Rocks: Elements, v. 9, no. 4, p. 273–279, doi: 10.2113/gselements.9.4.273.

Pysklywec, R.N., 2006, Surface erosion control on the evolution of the deep lithosphere: Geology, v. 34, no. 4, p. 225–4, doi: 10.1130/G21963.1.

Ranalli, G., 1995, Rheology of the Earth, Springer Science, 413 p.

Ranalli, G., and Murphy, D.C., 1987, Rheological stratification of the lithosphere: Tectonophysics, v. 132, no. 4, p. 281–295, doi: 10.1016/0040-1951(87)90348-9.

Reinecke, T., 1998, Prograde high- to ultrahigh-pressure metamorphism and exhumation of oceanic sediments at Lago di Cignana, Zermatt-Saas Zone, western Alps: Lithos, v. 42, no. 3-4, p. 147–189, doi: 10.1016/S0024-4937(97)00041-8.

Rosenberg, C.L., 2001, Deformation of partially molten granite: a review and comparison of experimental and natural case studies: International Journal of Earth Sciences, v. 90, no. 1, p. 60–76, doi: 10.1007/s005310000164.

Rosenberg, C.L., and Handy, M.R., 2005, Experimental deformation of partially melted granite revisited: implications for the continental crust: Journal of Metamorphic Geology, v. 23, no. 1, p. 19–28, doi: 10.1111/j.1525-1314.2005.00555.x.

Schmeling, H., Babeyko, A.Y., Enns, A., Faccenna, C., Funiciello, F., Gerya, T., Golabek, G.J., Grigull, S., Kaus, B.J.P., Morra, G., Schmalholz, S.M., and van Hunen, J., 2008, A benchmark comparison of spontaneous subduction models—Towards a free surface: Physics of the Earth and Planetary Interiors, v. 171, no. 1-4, p. 198–223, doi: 10.1016/j.pepi.2008.06.028.

Schmidt, M.W., Vielzeuf, D., and Auzanneau, E., 2004, Melting and dissolution of subducting crust at high pressures: the key role of white mica: Earth and Planetary Science Letters, v. 228, no. 1-2, p. 65–84, doi: 10.1016/j.epsl.2004.09.020.

Shatsky, V.S., Jagoutz, E., Sobolev, N.V., Kozmenko, O.A., Parkhomenko, V.S., and Troesch, M., 1999, Geochemistry and age of ultrahigh pressure metamorphic rocks from the Kokchetav massif (Northern Kazakhstan): Contributions to Mineralogy and Petrology, v. 137, no. 3, p. 185–205, doi: 10.1007/s004100050545.

Simon, G., and Chopin, C., 2001, Enstatite–sapphirine crack-related assemblages in ultrahigh-pressure pyrope megablasts, Dora-Maira massif, western Alps: Contributions to Mineralogy and Petrology, v. 140, no. 4, p. 422–440, doi: 10.1007/s004100000198.

Sizova, E., Gerya, T., and Brown, M., 2012, Exhumation mechanisms of melt-bearing ultrahigh pressure crustal rocks during collision of spontaneously moving plates: Journal of Metamorphic Geology, v. 30, no. 9, p. 927–955, doi: 10.1111/j.1525-1314.2012.01004.x.

Terry, M.P., Robinson, P., Hamilton, M.A., and Jercinovic, M.J., 2000, Monazite geochronology of UHP and HP metamorphism, deformation, and exhumation, Nordøyane, Western Gneiss Region, Norway: American Mineralogist, v. 85, no. 11-12, p. 1651–1664.

Torsvik, T.H., Smethurst, M.A., Meert, J.G., Van der Voo, R., McKerrow, W.S., Brasier, M.D., Sturt, B.A., and Walderhaug, H.J., 1996, Continental break-up and collision in the Neoproterozoic and Palaeozoic—a tale of Baltica and Laurentia: Earth-Science Reviews, v. 40, no. 3-4, p. 229–258, doi: 10.1016/0012-8252(96)00008-6.

van Roermund, H., 2009, Mantle-wedge garnet peridotites from the northernmost ultra-high pressure domain of the Western Gneiss Region, SW Norway: European Journal of Mineralogy, v. 21, no. 6, p. 1085–1096, doi: 10.1127/0935-1221/2009/0021-1976.

Vrijmoed, J.C., Van Roermund, H.L.M., and Davies, G.R., 2006, Evidence for diamond-grade ultra-high pressure metamorphism and fluid interaction in the Svartberget Fe–Ti garnet peridotite–websterite body, Western Gneiss Region, Norway: Mineralogy and Petrology, v. 88, no. 1-2, p. 381–405, doi: 10.1007/s00710-006-0160-6.

Warren, C.J., Beaumont, C., and Jamieson, R.A., 2008, Deep subduction and rapid exhumation: Role of crustal strength and strain weakening in continental subduction and ultrahigh-pressure rock exhumation: Tectonics, v. 27, no. 6, p. n/a–n/a, doi: 10.1029/2008TC002292.

Wilks, K.R., and Carter, N.L., 1990, Rheology of some continental lower crustal rocks: Tectonophysics, v. 182, no. 1-2, p. 57–77, doi: 10.1016/0040-1951(90)90342-6.

Xia, Q., Zheng, Y., and Zhou, L., 2008, Dehydration and melting during continental collision: Constraints from element and isotope geochemistry of low-T/UHP granitic gneiss in the Dabie orogen: Chemical Geology, v. 247, no. 1-2, p. 36–65, doi: 10.1016/j.chemgeo.2007.09.013.

- Partial melting of continental crust influences early collision dynamics.
- H2O-present partial melting is the most sensible reaction.
- Crustal partial melting and slab detachment both limit continental subduction.
- Melting at peak conditions may have occurred in most of UHP domains.

Material	k(T) (W/m/K)	H_r (W/m^3)	C_p (J/kg/K)	sin(ϕ)	C (MPa)	η_0 (Pa^n.s)	n	E_a (J/mol)	V_a (m3)
Sediments	0.64+ 807/(T+77)	1.50e-6	1000	0.15	1	1.97e17	2.3	1.54e5	0.8
U. O. C.	0.64+ 807/(T+77)	0.25e-6	1000	0.00	20	1.97e17	2.3	1.54e5	0.8
U. C. C.	0.64+ 807/(T+77)	1.00e-6	1000	0.45	20	4.97e20	3.1	2.43e5	1.2e-5
L. C. C.	1.18+ 474/(T+77)	0.25e-6	1000	0.45	20	4.97e20	3.1	2.43e5	1.2
L. O. C.	1.18+ 474/(T+77)	0.25e-6	1000	0.60	20	4.80e22	3.2	2.38e5	0.8
Dry M.	0.64+ 807/(T+77)	2.20e-8	1000	0.60	40	3.98e16	3.5	5.32e5	0.8
Serp &Wet M.	0.64+ 807/(T+77)	2.20e-8	1000	0.15	1	5.01e20	4.0	4.70e5	0.8

table 1

		T (K)
For the upper continental crust and sediments	**Water-present melting**	866.65+ 28.65/(P+0.097)at P< 2.2 GPa
		783+43.47*P at P≥ 2.2GPa
	Low T dehydration melting	916.65+ 8.58/(P+0.035)at P< 0.41 GPa
		$927.85+13.47*P +17.1*P^2-2.7*P^3$
		at P≥ 0.41 GPa
	High T dehydration melting	971+ 7.73/(P+0.0003)at P< 0.46 GPa
		$947+89.55*P -9*P^2+6.142*P^3$
		at P≥ 0.46 GPa
	Liquidus	1262+90*P
For lower continental crust and oceanic crust	**Solidus**	$972.6-70.36/(P+0.354)+77.81/(P+0.354)^2$
		at P< 1.6 GPa
		$935.4+3.486*P+6.243*P^2$ at P≥ 1.6 GPa
	Liquidus	1423.15+105*P
For ultramafics	**Solidus for wet peridotite**	1239.8+49.76/(P+0.323) at P< 2.4 GPa
		$1266.3-11.84*P+3.503*P^2$ at P≥ 2.4 GPa
	Solidus for dry peridotite	$1393.8+132.9*P-5.104*P^2$ at P< 1 GPa
		2212.4+30.8*(P-1) at P ≥ 1 GPa
	Liquidus	2017.15+114*P

table 2

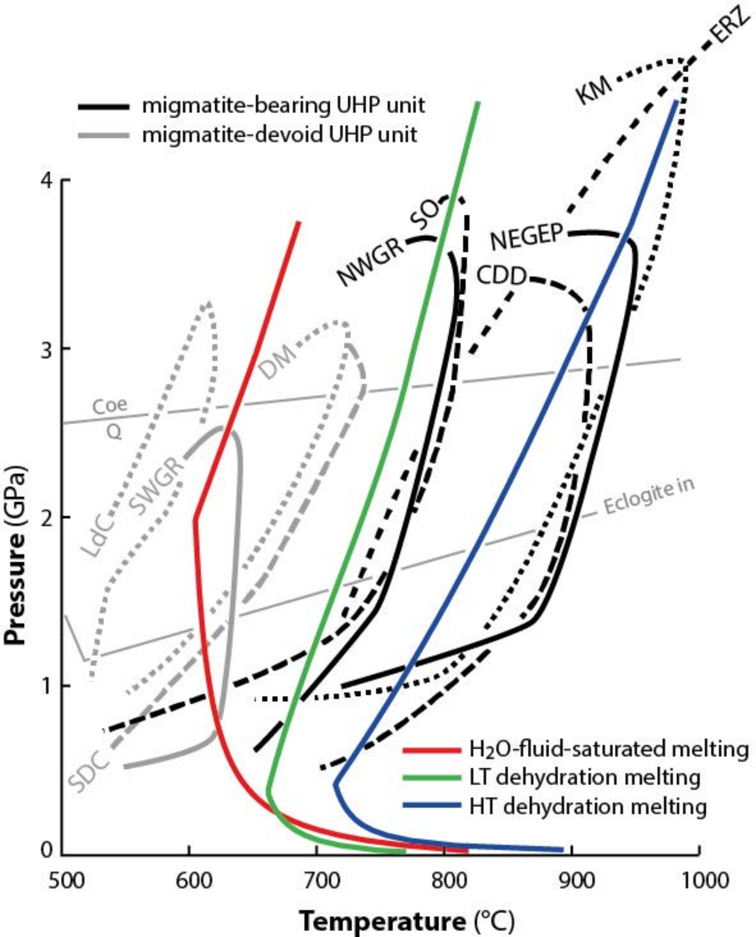
migmatite-bearing UHP unit
migmatite-devoid UHP unit
H2O-fluid-saturated melting
LT dehydration melting
HT dehydration melting
KM
ERZ
SO
NWGR
NEGEP
CDD
DM
Coe
Q
SWGR
LdC
SDC
Eclogite in
Pressure (GPa)
Temperature (°C)
0
1
2
3
4
500
600
700
800
900
1000

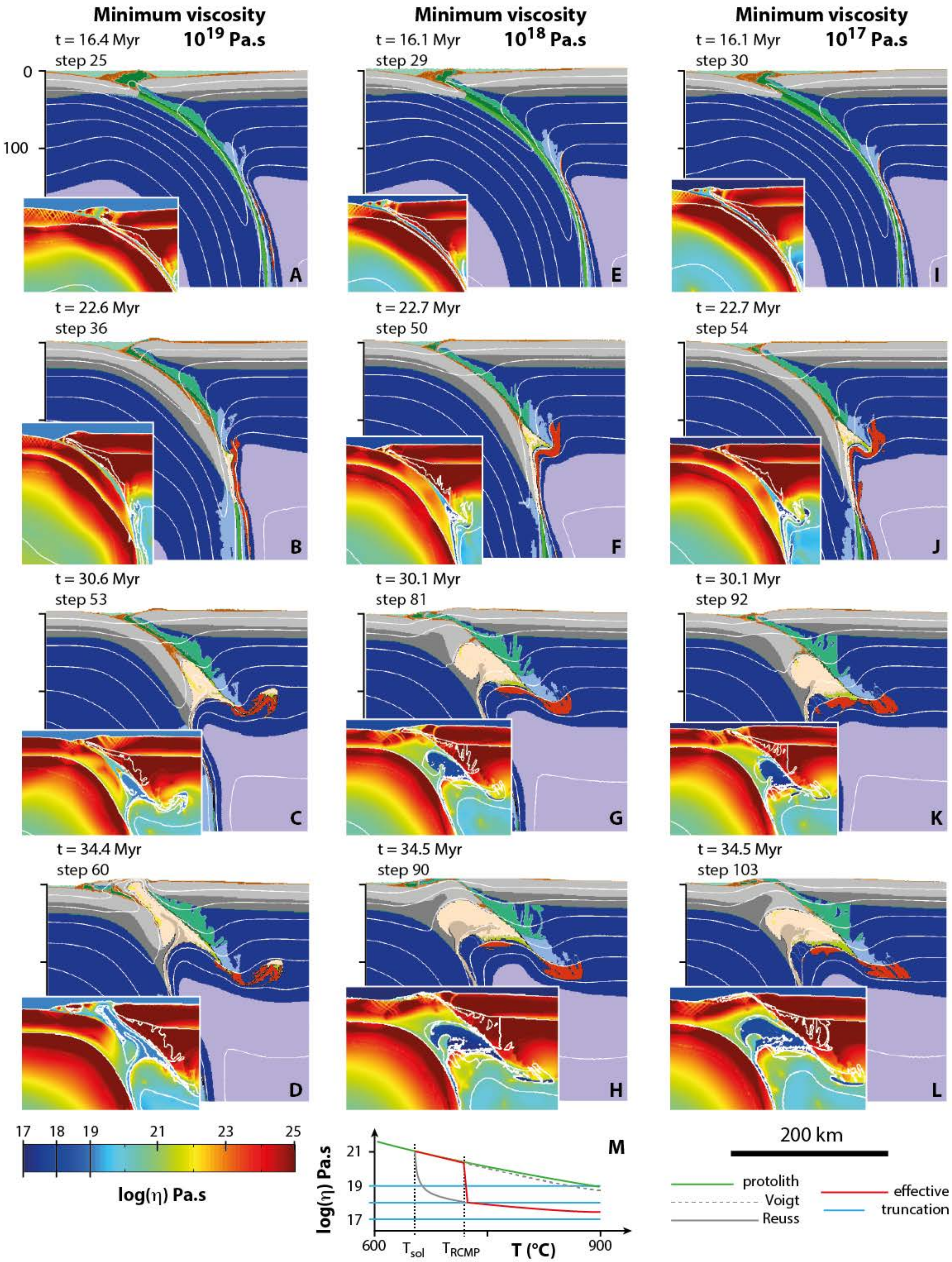

Minimum viscosity
10^{19} Pa.s
Minimum viscosity
10^{18} Pa.s
Minimum viscosity
10^{17} Pa.s
t = 16.4 Myr
step 25
t = 16.1 Myr
step 29
t = 16.1 Myr
step 30
0
100
A
E
I
t = 22.6 Myr
step 36
t = 22.7 Myr
step 50
t = 22.7 Myr
step 54
B
F
J
t = 30.6 Myr
step 53
t = 30.1 Myr
step 81
t = 30.1 Myr
step 92
C
G
K
t = 34.4 Myr
step 60
t = 34.5 Myr
step 90
t = 34.5 Myr
step 103
D
H
L
17 18 19 21 23 25
log(η) Pa.s
M
log(η) Pa.s
21
19
17
600
T_{sol}
T_{RCMP}
T (°C)
900
200 km
protolith
Voigt
Reuss
effective
truncation

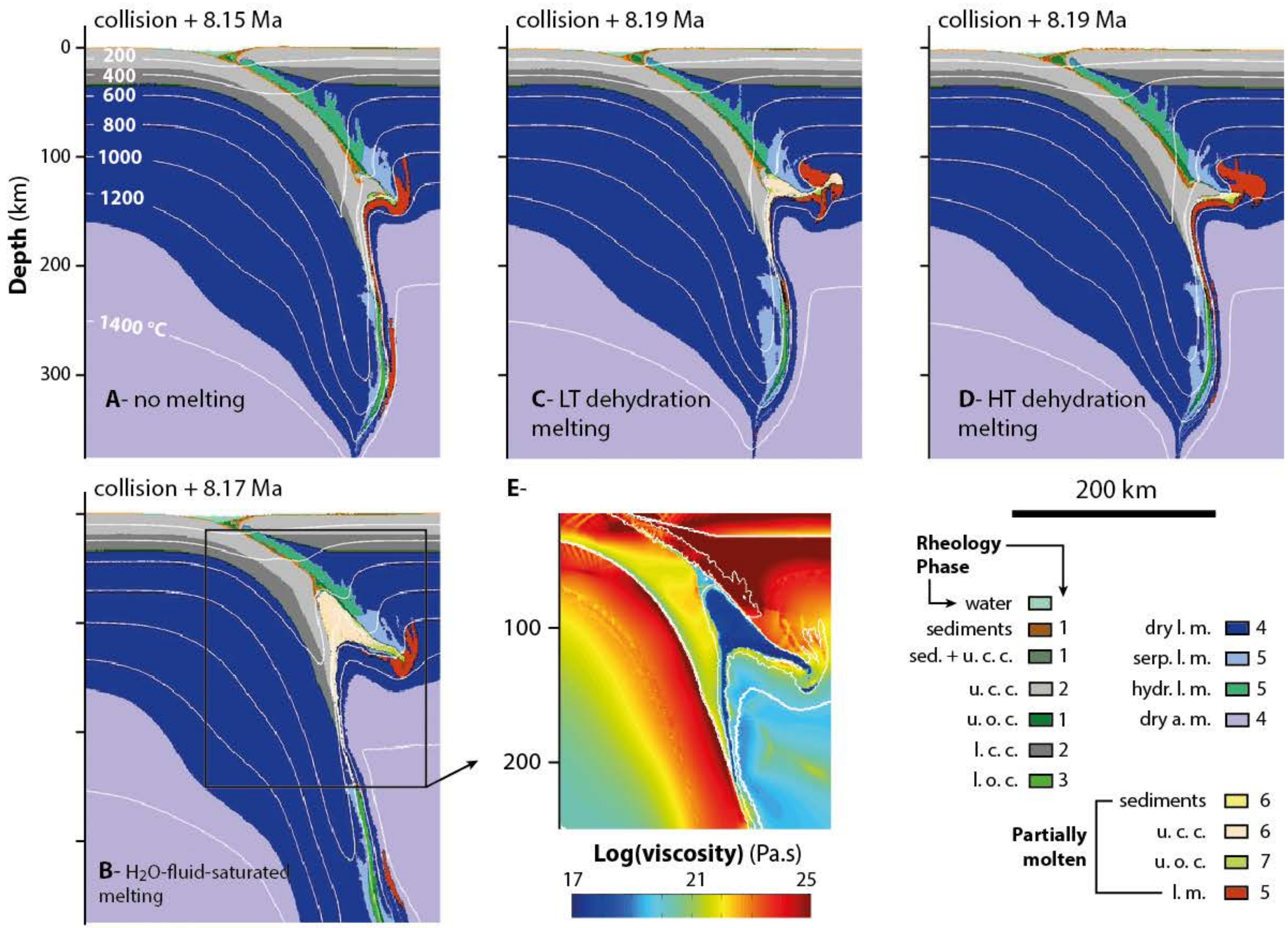

collision + 8.15 Ma
collision + 8.19 Ma
collision + 8.19 Ma
Depth (km)
0
100
200
300
200
400
600
800
1000
1200
1400 °C
A- no melting
C- LT dehydration melting
D- HT dehydration melting
collision + 8.17 Ma
B- H2O-fluid-saturated melting
E-
100
200
Log(viscosity) (Pa.s)
17
21
25
200 km
Rheology
Phase
water
sediments 1
sed. + u. c. c. 1
u. c. c. 2
u. o. c. 1
l. c. c. 2
l. o. c. 3
dry l. m. 4
serp. l. m. 5
hydr. l. m. 5
dry a. m. 4
Partially molten
sediments 6
u. c. c. 6
u. o. c. 7
l. m. 5

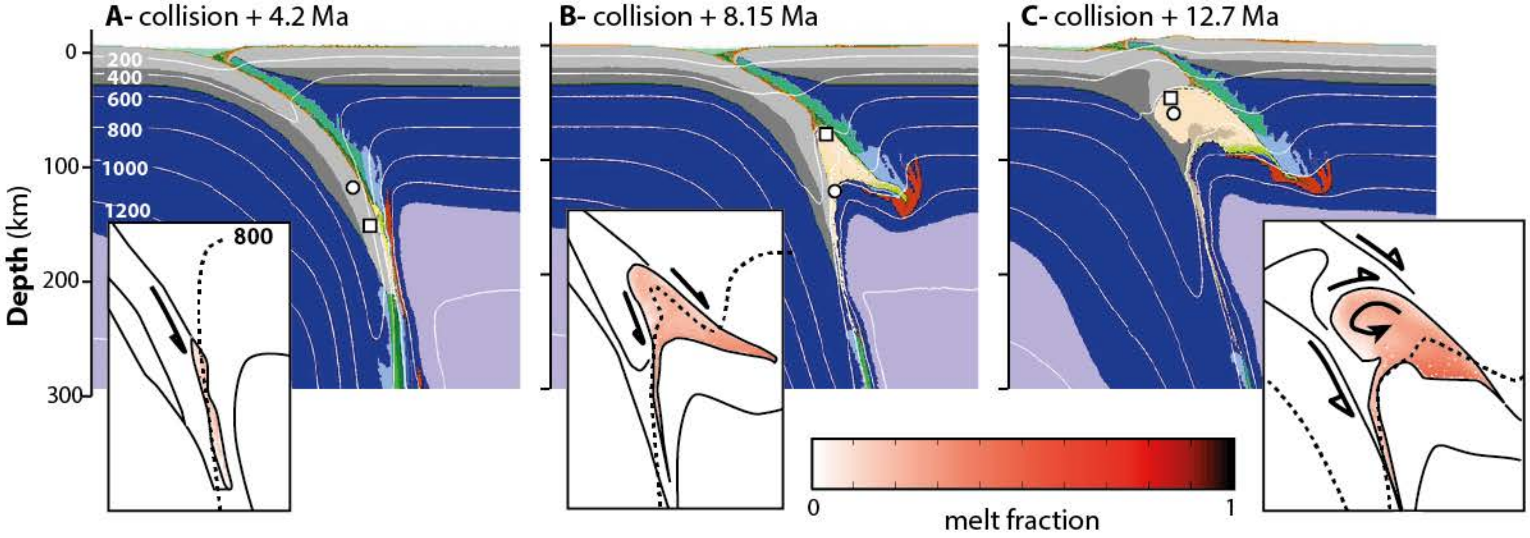

A- collision + 4.2 Ma
B- collision + 8.15 Ma
C- collision + 12.7 Ma
Depth (km)
0
100
200
300
200
400
600
800
1000
1200
800
0
melt fraction
1

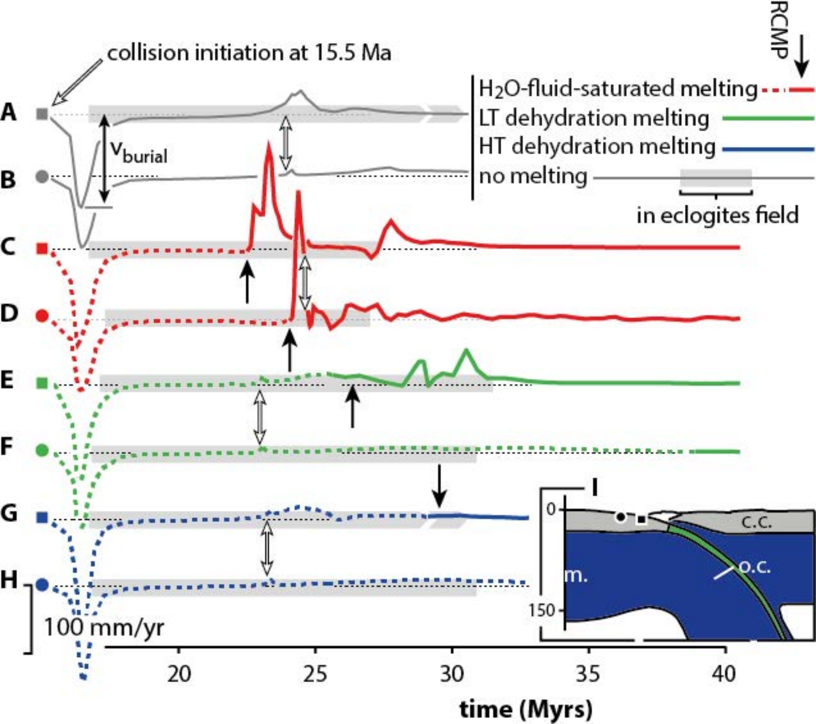

RCMP
collision initiation at 15.5 Ma
H2O-fluid-saturated melting
LT dehydration melting
HT dehydration melting
no melting
in eclogites field
A
B
C
D
E
F
G
H
I
v burial
100 mm/yr
0
150
c.c.
o.c.
m.
20
25
30
35
40
time (Myrs)

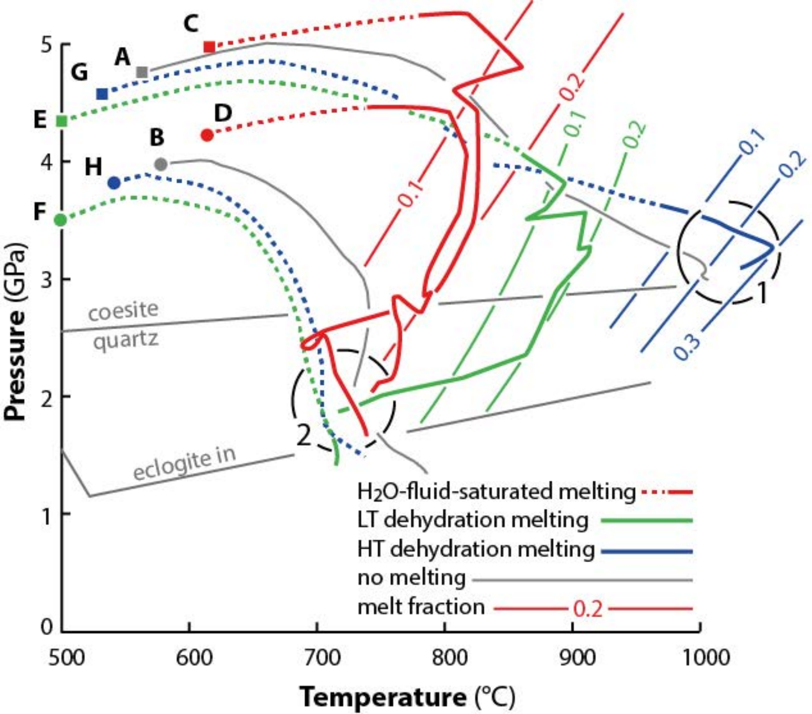

C
A
G
E
D
B
H
F
5
4
3
2
1
0
Pressure (GPa)
coesite
quartz
eclogite in
0.1
0.2
0.1
0.2
0.1
0.2
0.1
0.3
1
2
H2O-fluid-saturated melting
LT dehydration melting
HT dehydration melting
no melting
melt fraction 0.2
500
600
700
800
900
1000
Temperature (°C)

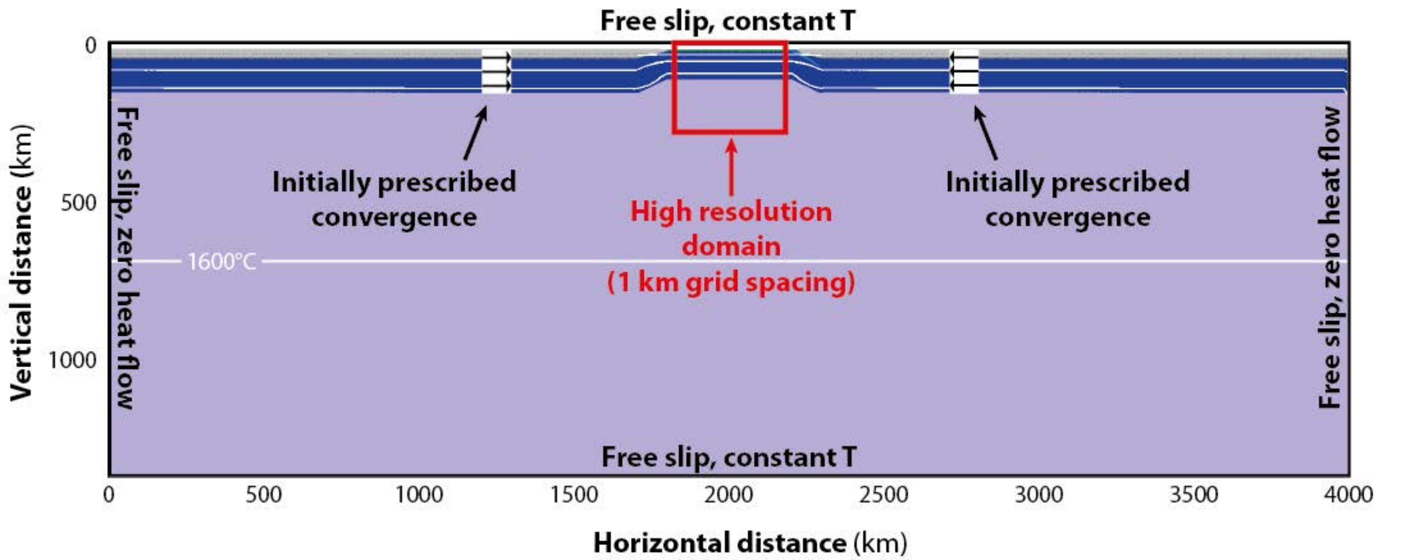
Free slip, constant T
0
500
1000
Vertical distance (km)
Free slip, zero heat flow
Initially prescribed convergence
High resolution domain (1 km grid spacing)
Initially prescribed convergence
Free slip, zero heat flow
1600°C
Free slip, constant T
0
500
1000
1500
2000
2500
3000
3500
4000
Horizontal distance (km)